Advances in Nano Research, *Vol. 3, No. 3 (2015) 143-168*
DOI: http://dx.doi.org/10.12989/anr.2015.3.3.143

Crack growth prediction and cohesive zone modeling of single crystal aluminum-a molecular dynamics study

Vijay Kumar Sutrakar*[1,2], N. Subramanya[1,3] and D. Roy Mahapatra[3]

[1]*Aeronautical Development Establishment, Defence Research and Development Organization, New Thipasandara Post, Bangalore, 560075, India*
[2]*Presently at Aeronautical Development Agency, Post Box No. 1718, Vimanapura Post, Bangalore, 560017, India*
[3]*Department of Aerospace Engineering, Indian Institute of Science, Bangalore 560012, India*

(Received July 3, 2015, Revised December 7, 2015, Accepted December 8, 2015)

Abstract. Initiation of crack and its growth simulation requires accurate model of traction – separation law. Accurate modeling of traction-separation law remains always a great challenge. Atomistic simulations based prediction has great potential in arriving at accurate traction-separation law. The present paper is aimed at establishing a method to address the above problem. A method for traction-separation law prediction via utilizing atomistic simulations data has been proposed. In this direction, firstly, a simpler approach of common neighbor analysis (CNA) for the prediction of crack growth has been proposed and results have been compared with previously used approach of threshold potential energy. Next, a scheme for prediction of crack speed has been demonstrated based on the stable crack growth criteria. Also, an algorithm has been proposed that utilizes a variable relaxation time period for the computation of crack growth, accurate stress behavior, and traction-separation atomistic law. An understanding has been established for the generation of smoother traction-separation law (including the effect of free surface) from a huge amount of raw atomistic data. A new curve fit has also been proposed for predicting traction-separation data generated from the molecular dynamics simulations. The proposed traction-separation law has also been compared with the polynomial and exponential model used earlier for the prediction of traction-separation law for the bulk materials.

Keywords: molecular dynamics simulations; single crystal; crack growth; stresses; traction-separation law

1. Introduction

The process of fracture mechanics has attracted considerable attention since last few decades. Even though continuum mechanics has been very successful in predicting material behaviors at macroscopic scale, the atomic simulations has proven to be a most indispensable tool in forecasting response of the material subjected to extreme stresses. Despite achievement of significant milestones in the development of continuum mechanics of fracture (Griffith 1921, Irwin 1948, Irwin 1956, Dugdale 1960, Irwin 1957, McClintock 1968, Rice and Rosengren 1968,

*Corresponding author, Ph.D., E-mail: vijay.sutrakar@gmail.com

http://www.techno-press.com/?journal=anr&subpage=7 ISSN: 2287-237X (Print), 2287-2388 (Online)

Westergaard 1939, Williams 1957) the complex fracture mechanism occurring at atomistic level is not completely understood. However, it is well known that the observable fracture phenomenon at macroscopic level is an outcome of various events occurring at micro- and nano- scale. The smallest scale could be the breaking of bonds between the atoms as the crack propagates. In this direction, Molecular Dynamics (MD) Simulations have played a vital role in micro-/nano- scale modeling of material and to track the individual atom of interest. Studies carried out by MD simulation helps in accurate modeling and estimation of cohesive zone (Krull and Yuan 2011, Zeng and Li 2010, Tvergaard 2001, Yamakova *et al*. 2006, Tomar *et al*. 2004, Kubair and Geubelle 2003, Dantuluri *et al*. 2007), fracture mechanism occurring at the interface of two materials (Zhou *et al*. 2009). Atomic simulations not only helps to accurately estimate the stress field in the vicinity of crack tip, it also aids in better understanding of fracture dependency on crystallographic loading orientation, initial nano-void volume fraction, geometry, temperature, strain rate etc. (Abraham and Broughton 1998, Holland and Marder 1999, Rosch *et al.* 2006, Bringa *et al*. 2010, Wu and Yao 2012).

In order to perform an accurate cohesive zone modeling, it is important to first understand the behavior of crack initiation and crack growth accurately so that the accurate cohesive law could be implemented. Even though most of the atomistic studies of fracture behavior at the nano-scale have been focused on investigation of brittle fracture events, there are a few discoveries that provide an analysis and understanding of nano-scale ductile fracture events, which is indeed a result of void formation ahead of the crack tip, void growth and link up with the main crack (Garrison and Moody 1987, Tai and Yang 1986, Xu and Deng 2008, Bhatia *et al.* 2012, Potirniche *et al.* 2006, Roy *et al*. 1981). It is also shown that ductile fracture is an end result of sequence of three processes (i) void formation, (ii) void growth, and (iii) coalescence (McClintock 1968, Thomason 1968). However, predicting failure in ductile material requires thorough understanding of complex process of micro structural damage evolution and progression wherein the void forms, grow, and link up with the main crack. Xue and Wierzbicki (2008) have also modeled the ductile fracture mechanism using damage plasticity theory.

In the present work, nano-scale single crystal aluminum with a stationary single edge crack, subjected to remote mode-I loading has been considered. The aim of the present study is to identify the several nano-scale events that lead to fracture in aluminum, and to figure out the dependency of atomic scale fracture events on atomic stresses. To study the nano-scale fracture behavior and investigate the effect of stress fields on the fracture process, several atomistic stress definitions have been employed in the present work. It includes atomic stress, average atomic stress, hydrostatic atomic stress, and Von-Mises atomic stress based on the average atomic stress. Next, an attempt has been made to develop an accurate traction separation law which is one of the main aims of the present paper. It is also very important to understand the crack initiations and crack growth accurately so that an accurate traction - separation data could be generated from MD. In this direction, an attempt has been made to understand the stability of the crack initiation and crack growth and its impact on the traction - separation data. Also, the MD traction - separation data has been compared with the existing polynomial (Needleman 1987) and exponential form (Needleman 1990) of traction - separation law used for bulk material modeling. It is shown that both the polynomial as well as exponential form of fit used for macroscopic studies does not match well with the MD traction - separation data of single crystal Al. However, the effect of crystal orientation, different initial temperature, and different class of FCC single crystal are still an open area of research. Finally, a new curve fit for the present set of MD traction - separation data has also been proposed.

2. Modeling setup and simulation methodology

In this section, details of modeling setup and simulation methodology adopted to carry out MD simulations are discussed. Firstly, a brief discussion of MD techniques and interatomic potentials utilized in the present study is presented. Next, the details of model geometry and boundary conditions are presented. Finally, discussions on several atomistic stress definitions employed in this work are provided to understand the nano-scale fracture behavior and to investigate the effect of stress fields on various fracture process.

2.1 Molecular dynamics (MD) and interatomic potential details

MD simulations predict the motion of an atomistic system using the equations of motion governed by Newton's second law. The governing equation for an atom *i* in the system is given by $\mathbf{F}_i = \mathrm{m}_i\ddot{\mathbf{r}}_i$, where m_i and $\mathbf{r}_i$ are the mass and position of atom *i*, respectively. $\ddot{\mathbf{r}}_i$ is the double time derivative of $\mathbf{r}_i$, and $\mathbf{F}_i$ is the total interaction force on atom *i* by its neighbors. In MD simulations the total interaction force $\mathbf{F}_i$ on atom *i* by its neighbors is determined by the gradient of the total interatomic potential E of the atomic system through $\mathbf{F}_i = -\overline{\nabla}_i \mathrm{E}\,(\mathbf{r}_1, \mathbf{r}_2, \mathbf{r}_3, \ldots \mathbf{r}_n)$ where $\mathbf{r}_1, \mathbf{r}_2, \mathbf{r}_3, \ldots \mathbf{r}_n$ are the positions of the atoms in an atomic system of *n* atoms. In this work, the most common numerical time integration method of Velocity Verlet algorithm is used (Swope *et al.* 1982). Many forms of reliable interatomic potentials with various levels of complexity and accuracy have been proposed in the recent past for a range of materials based on large set of experimental, empirical, semi-empirical, and ab-initio data.

Among these potentials, the embedded atom method (EAM) potential (Daw and Baskes 1984) is one of the most commonly used potentials for FCC metallic materials. The EAM potential describes the total energy E for a system of atoms as

$$\mathrm{E} = \sum_i^N \mathrm{F}_i\,(\bar{\rho}_i) + \frac{1}{2}\sum_{j\neq i}^N \boldsymbol{\emptyset}_{ij}\left(\mathbf{r}_{ij}\right) \tag{1}$$

where the summations in Eq. (1) extend over the total number of atoms *N* in the system. F_i is the embedded energy as a function of the host electron density $\overline{\rho}_i$ induced at site *i* by all other atoms in the system, and $\boldsymbol{\emptyset}_{ij}$ is the pair potential as a function of the distance $\mathbf{r}_{ij}$ between atom *i* and *j* . The electron density is given by

$$\bar{\rho}_i = \sum_{j\neq i}^N \rho_j(\mathbf{r}_{ij}) \tag{2}$$

where $\rho(\mathbf{r})$ is the electron density function assigned to an atom *j*. EAM potential developed by Liu *et al.* (2004) is employed in the present work which is derived from density functional theory calculations. The potential predicts more accurately crystal defects and dislocations dynamics of aluminum crystals. A large number of crack growth related studies are already performed in recent past utilizing this potential (Krull and Yuan 2011, Xu and Deng 2008).

2.2 Model geometry and boundary conditions

In this work, a constrained three dimensional model consist of FCC single crystal of aluminum with a single edge crack is employed to investigate crack initiation and crack growth behavior (similar model has also been considered in the recent past by Krull and Yuan (2011), Xu and Deng (2008)). The size of the model considered is 125a×70a×6a (50.51 nm×30.3 nm×2.42 nm), where *a*

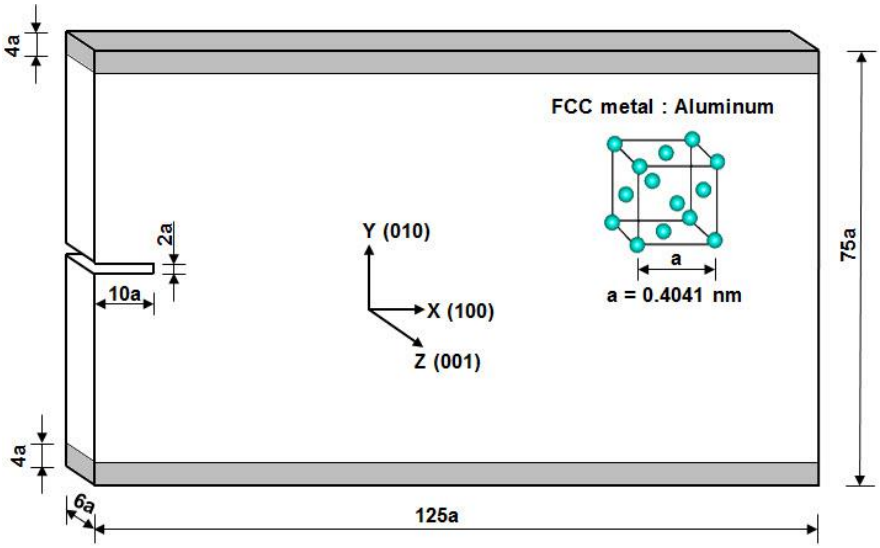

Fig. 1 Crack specimen geometry of a FCC single crystal Al considered for MD simulations

(a=0.4041 nm) is the lattice constant of aluminum, as shown in Fig. 1. The corresponding MD sample consists of ~ 2,20,000 atoms. All the simulations are carried out with 50 *Intel* core at 3.0 GHz Processors in parallel utilizing Linux. An approximate time of 1-5 days (depending on different simulation conditions considered in the present paper) used to takes for the completion of one run. The model thickness is considered to be greater than 4a, to diminish additional size effects (Horstemeyer and Baskes 1999). Because of the use of the periodic condition and a small number of lattice layers in the thickness direction (to limit the amount of computation), this 3D model is called a constrained 3D model (Xu and Deng 2008). Also, periodic boundary condition along the thickness of the specimen ensures the plane strain condition for the simulation. The lattice is orientation such that *X*-direction is along [100], *Y*-direction is along [010], and *Z*-direction is along [001].

An artificial crack is created in the left central region of the geometry by removing atoms of those regions, as shown in Fig. 1. In the model, the two faces of the single edge crack are parallel to the <010> plane and are a distance of 2a (0.808 nm) apart, and the initial crack length is equal to 10a (4.04 nm). Energy minimization of the structure is performed (at T=0 K) utilizing Conjugate Gradient method. After the energy minimization, the top and bottom boundary of the structure (consists of distance 4a) is held fixed, as shown in Fig. 1. The displacement in the *X*-direction along the right boundary is constrained to zero in order to limit boundary effects. Following the energy minimization process, the system is equilibrated at a given temperature of ~0 *K* using the Nose-Hoover thermostat (Nose 1984, Hoover 1985) for 50 picosecond (ps) with a time step of 0.001 ps. All simulations are performed using an MD code called LAMMPS (Plimpton 1995, LAMMPS 2013). Next, the system is stretched in the *Y* direction along the top boundary with a displacement controlled loading while the bottom boundary is held stationary. After the application of displacement controlled loading of a given duration of 1ps, the system is relaxed for a particular time period. Six different relaxation time periods of 1ps, 10ps, 20ps, 30ps, 40ps, and 50ps are considered between two consecutive loading steps to see the stability of crack growth. After this fixed interval of relaxation time period, further displacement controlled loading is

applied for further growing the crack and this process continues till the complete fracture is observed in the sample. Finally, the deformed configuration of the system is predicted using MD simulation. All simulations are preformed at temperature of ~0 *K* using a method to rescale the velocities of the atoms to avoid any thermal activation. This assumption diminishes effects of atom vibration and will not affect our discussions. However, the effect of temperature grow during the displacement controlled loading is still an open area of research.

2.3 Atomic stresses

The atomic stress at an atom *i* is a stress quantity at the atomic scale. It is a strength measurement of the interatomic interactions of the atom with its neighboring atoms. This stress tensor is defined in component form as (Zhou 2003)

$$\sigma_{\alpha\beta}(i) = -\frac{1}{2\mathrm{V}_i}\sum_{j\neq i}^{N} \mathbf{F}_{\alpha}(i,j)\,\mathbf{r}_{\beta}(i,j) \tag{3}$$

where $\alpha, \beta = x, y, z$. N is the number of atoms in a region around atom i within an EAM potential cut-off distance (which is 6.063 Å for Al), $\mathbf{F}_{\alpha}(i,j)$ is the vector component form of the interaction force exerted by atom j on atom i, $\mathbf{r}_{\beta}(i,j)$ is the vector component form of the relative position from atom j to atom i, and V_i is the volume of atom i given by $\mathrm{V}_i = \frac{4}{3}\,\pi\,\mathbf{R}_i{}^3$, where $\mathbf{R}_i$ is the radius of the atom i. Taking an average of the atomic stress over the volume around atom i within the cut-off distance, the average atomic stress at an atom i is defined as

$$\sigma_{\alpha\beta}^{\mathrm{avg}}(i) = \frac{1}{N}\sum_{j=1}^{N}\sigma_{\alpha\beta}(j) \tag{4}$$

where $\sigma_{\alpha\beta}(j)$ is the atomic stress at atom j. Analogous to stress definitions at a point in a continuum, the mean (hydrostatic) average atomic stress $\sigma_{\mathrm{mean}}(i)$ and the Von-Mises effective average atomic stress $\sigma_{von}(i)$ at an atom i can be defined based on the average atomic stress at the atom as

$$\sigma_{\mathrm{mean}}(i) = \frac{1}{3}\left[\sigma_{xx}^{\mathrm{avg}} + \sigma_{yy}^{\mathrm{avg}} + \sigma_{zz}^{\mathrm{avg}}\right] \tag{5}$$

$$\sigma_{\mathrm{von}}(i) = \sqrt{\frac{1}{2}\left[\left(\sigma_{xx}^{\mathrm{avg}} - \sigma_{yy}^{\mathrm{avg}}\right)^2 + \left(\sigma_{yy}^{\mathrm{avg}} - \sigma_{zz}^{\mathrm{avg}}\right)^2 + \left(\sigma_{zz}^{\mathrm{avg}} - \sigma_{xx}^{\mathrm{avg}}\right)^2 + 6\left(\sigma_{xy}^{\mathrm{avg}^2} + \sigma_{yz}^{\mathrm{avg}^2} + \sigma_{zx}^{\mathrm{avg}^2}\right)\right]} \tag{6}$$

2.4 Evaluation of traction – separation over the damage zone

The cohesive zone model is introduced in the literature to study failure of ductile materials. The main idea of the cohesive zone model is to reduce the finite fracture process zone ahead of the crack tip, where material damage occurs, to a strip with zero thickness. The damage evolution in the region is characterized by the relationship between the traction (T) and separation (δ), i.e., the traction–separation law. Since, it is introduced for a fictive zone, which cannot directly be found in reality, hence, formulation of the traction–separation law becomes a key issue in development and verification of the cohesive model. Atomistic simulations are based on atomic potentials and can provide information of inter-relations between these variables and find a new way for homogenization of the discrete damage process in micro/nano-scale to the macro-scale in

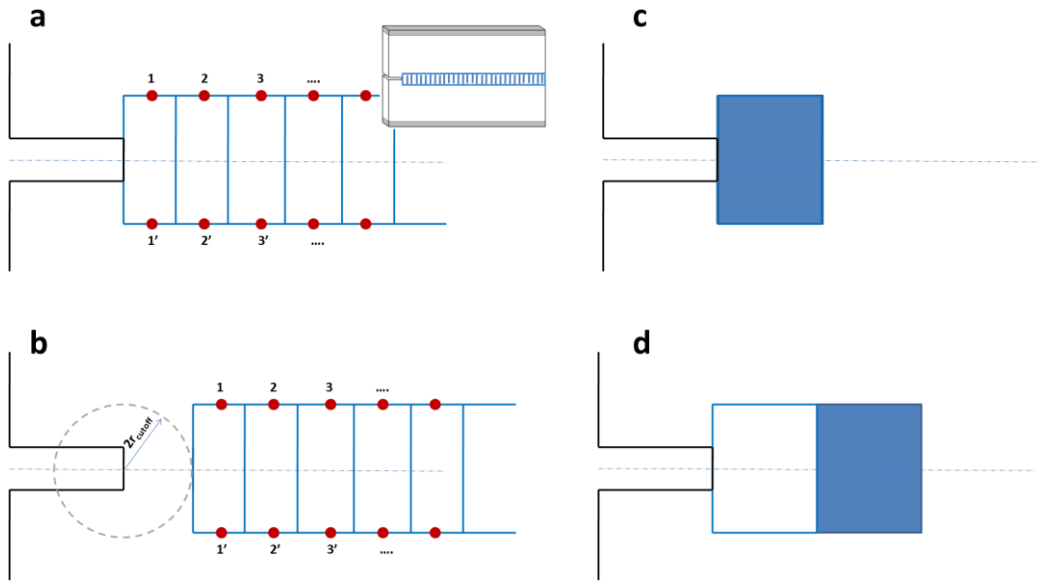

Fig. 2 A schematic representation of zoomed view of Fig. 1 near the crack tip is shown here. (a) Cell introduced for evaluating the averaged atomic tensile stress, averaged hydrostatic stress, averaged Von-Mises stress, and averaged traction-separation data. The initial system is divided into N cells for performing averaging. In each cell two atoms, one at top side and another at bottom side are identified to calculate the separation as marked in red. (b) The cell is introduced from twice the cut-off distance ($2r_{cufoff}$) from the initial crack tip to study the effect of surface on the traction - separation law. (c) Region -1 and (d) Region -2 considered for the computation of stress triaxiality

engineering materials (Krull and Yuan 2011).

In order to evaluate the traction-separation over a damage zone, a method similar to what is proposed by Krull and Yuan (2011) has been utilized in the present paper, as shown in Fig. 2. In this method, after the energy minimization, the initial system is divided into *N* vertical cell along the *y*-axis with finite thickness of +/– 4*a* (*a*=lattice constant) along x-axis. An approximate width of 10Å is considered for individual vertical cell (along the *x*-axis). In each cell, one atom from the upper most regions and another one from the bottom most regions have been considered to track the crack trajectory that will finally lead to the prediction of separation. The atom ids of all the atoms inside a cell is stored separately and traced during the crack growth process for the calculation of averages stress quantities. This will lead to the averaged traction quantity for separation of a given cell.

3. Identification of crack growth (threshold potential energy vs. CNA)

In the recent past, many attempts have been made to identify crack growth of single crystal utilizing molecular dynamics simulations. For example, Xu and Deng (2008) have shown effective crack length during the crack growth study of single crystal Al. An effective crack with the mathematical crack tip being at the physical crack tip (when there is no void ahead of the crack tip) or at the forward tip of the leading void (when one or more voids exist ahead of the physical

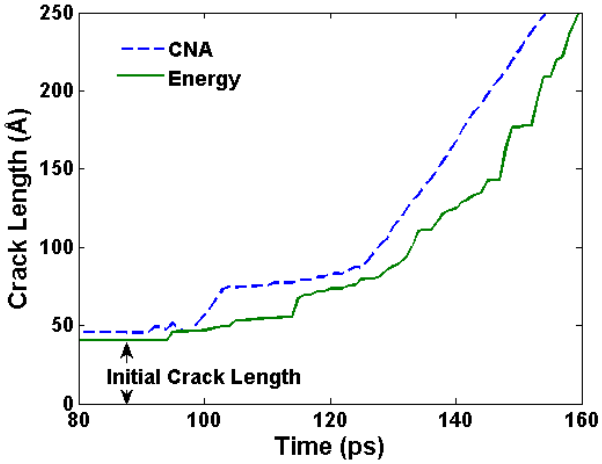

Fig. 3 Crack length (Å) v/s Time (ps) plot for CNA and energy approach for predicting crack growth. The length of initial artificial crack considered in the present study is also marked

crack tip) is considered for extracting crack growth. The exact mechanism of extracting crack growth data is not discussed in Xu and Deng (2008). However, the data presented in the Fig. 3 of present paper indicates that energy based approach for extraction of data for predicting crack growth has been considered in Xu and Deng (2008). The details of the energy based approach considered in the present paper will be provided in subsequent section. Zhou *et al.* (2008) have also shown the dynamic variation of crack length during simulations and it is used for examine the correlation between the observed stress–strain curves and fracture. It is well known that atoms at the cracked surface have significantly higher energy than those in the bulk. Zhou *et al.* (2008) have used threshold energy to determine the crack length. In order to calculate threshold energy, an average potential energy was calculated over all atoms in each of the regions (Zhou *et al*. 2008). If this average energy was larger than the threshold energy, the corresponding region was counted as cracked. The similar concept of crack detection was used in Zhou *et al*. (2009) for studying the effects of elastic constant mismatch for brittle interfacial fracture simulations under mixed mode loading condition.

Ren *et al.* (2012), Wu and Yao (2012) have also used the similar approach in which the crack tip position is determined by searching the surface atom in the vicinity of crack tip on the basis of potential energy criterion. By choosing an appropriate threshold value of the potential energy, the surface atom closest to the crack tip region has been extracted and the crack tip position changing with time has been obtained. A similar concept has also been used in (Paliwal and Cherkaoui 2013) for studying mixed mode cohesive zone law while considering non-planar crack growth. Different energies including a threshold value (u_t), average potential energy (u_s), and bulk potential energy (u_b), and bonded interface energy (u_i) and correlations amongst them are considered for the identification of crack growth.

The above study indicates that the identification of accurate threshold values of potential energy is a cumbersome task. It is also observed by the present authors that the threshold energy method requires cross-checking at every loading steps for the prediction of accurate crack growth and for the confirmation whether the threshold value of energy selected is correct or not (as the energies of surface atoms keep on fluctuate). In the present paper, two different criterion for the

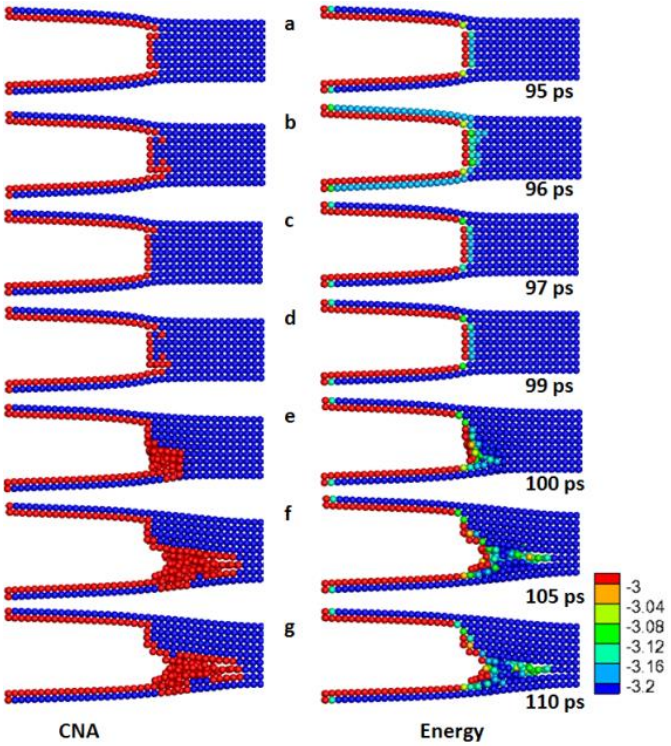

Fig. 4 CNA v/s Energy contours with varying time steps near the crack tip region. The blue atoms in CNA contour shows perfect FCC lattice and red atoms are corresponds to an unknown lattice structure and corresponds to surface atoms and dislocations. The energy plot shows the variations in potential energy (in eV) with blue atom as the energy of bulk atoms

identification of crack growth are studied and compared, i.e., (i) threshold potential energy and (ii) common neighbor analysis (CNA). In the case of first method, value of potential energy at the initial crack tip is considered as the threshold and the same value of potential energy is tracked with growing crack for the identifications of crack tip. The pattern of crack growth observed with this method as shown in Fig. 3 is similar to what is reported in Xu and Deng (2008) (refer Fig. 15 of Xu and Deng (2008) for further details). During the process of crack growth identifications, it is observed that this method does not work well for the identifications of crack tip due to the following two reasons. Firstly, localized defects for example voids formation, which are not at the crack tip (could be ahead/behind of actual crack tip) may have the same threshold value of potential energy. Secondly, it is also observed by the authors that the potential energy at the crack tip may have lower values as compared to the threshold potential energy with growing crack.

In order to remove the above mentioned artifacts of potential energy approach, a modified scheme is adopted in the potential energy approach itself. In the modified scheme, the region behind of crack tip (region behind threshold potential energy) is neglected in the next step of loading. In this way, localized defect, if any, (that is in actual behind of crack tip locations) which has the same threshold potential energy was able to remove during the crack growth computations. However, this scheme has other drawbacks, i.e. it is not able to capture the closure of the crack tip, if occurs during the process of crack growth may be either due to stress relaxation or shape

memory recovery of materials. In order to make the process of identification of crack growth simpler, a different technique based on common neighbor analysis (CNA) technique is studied. It is important to mention here that CNA technique is used extensively in the literature in past for the identifications of defects and free surfaces in nano-crystalline materials. The concept of CNA is introduced by Honeycutt and Andersen (1987) for determining the equilibrium structure of small clusters of Lennard- Jones atoms. Jonsson and Andersen (1988) used the same technique to study the structures produced by cooling Lennard- Jones fluids to below the glass transition. Clarke and Jonsson (1993) used a slight different version of the CNA to investigate the densification and the icosahedral ordering of hard-sphere packing. Faken and Jonsson (1994) used the same version of CNA in combination with 3D computer graphics to study the crystal nucleation in a molten copper slab. The CNA has also been useful in the investigation of the microstructure of liquid and amorphous Ni (Garzón and Amarillas 1996), small Au clusters (Amarillas and Garzón 1996, Li *et al.* 2000), metallic nano contacts (Sørensen *et al.* 1998), grain boundaries (Schiøtz 1997a, b), dislocation processes in nano-crystalline aluminum (Yamakov 2002) liquid and super-cooled tantalum (Jakse and Pasturel 2004), liquid and super-cooled copper (Ganesh and Widom 2006), and metallic glasses (Yavari *et al.* 2007). The use of CNA makes dislocations, grain boundaries, and stacking faults visible in the simulation. This efficient and convenient technique serve well in the visualization and interpretation of datasets obtained from MD simulations of simple systems with fcc, hcp, or bcc structure. However, no attempt has been made for the identification of crack growth utilizing this approach.

CNA technique identifies the local structure in atomic systems by using information about the mutual relation between neighbors of atoms pair. In this technique, the surface atoms show an unknown lattice, which is due to the fact that the surface atoms do not have the same neighbors of atom pairs (due to the free surfaces) compared to the other part of the structure which has perfect FCC lattice. The atoms are shown in blue in Fig. 4(a) which has perfect FCC crystal structure (having CNA patterns 1) and the atoms shown in red are the atoms at the free surfaces (having CNA patterns 5). For further details on the CNA patterns, refer (LAMMPS 2013, Faken and Jonsson 1994). In order to monitor the crack growth, the position of CNA=5 is monitored along the crack length axis. As the crack started growing, the CNA value shifted from the free surface of the crack tip to the inside (refer Fig. 4 for further details) and CNA of perfect lattice (CNA =1) changes into 5. Hence, the accurate crack tip is identified with growing crack. Also, if any closure of the crack happens, this method is able to predict it accurately, as it occurs during 96ps to 97ps in the present simulation, as also shown in Fig. 4. In the present work, CNA has been studied at 0K; however, the effect of CNA on the crack prediction with temperature needs to be studied.

A detailed comparison between the threshold potential energy and CNA technique with growing crack is presented in Fig. 4. It can be seen that the crack is slightly opened up from both the top and bottom end of the crack tip, as marked by red atoms in CNA and shown in snapshot '*a*' of Fig. 4. On the other side, the threshold potential energy that is not able to capture the crack initiations as the potential energy observed in those regions are lower than the threshold values. The similar behavior is shown in snapshot '*b*' of Fig. 4 where CNA capture the crack initiation accurately. In the snapshot '*c*' of Fig. 4, it is observed that the crack is closing at that particular step of loading (it can be seen in both the CNA as well as energy approach). However, the threshold potential energy still shows the location of crack growth at the initial crack tip locations only. On the other hand, the CNA technique shows the crack growth reductions during the closure of crack tip (also demonstrated in Fig. 3 at 97ps where a sudden drop in crack growth is shown for CNA technique). In the snapshots '*d*' and '*e*' of Fig. 4, it can be seen that the crack is started

growing and both the technique shows increase in crack length, however, still the energy approach shows smaller length of crack compared to the CNA technique (also demonstrated in Fig. 3). In the snapshots '*f*' and '*g*' of Fig. 4, it can be seen that the crack is further grown and it leads to localized defects which has potential energy much lower than the threshold value of potential energy. However, the CNA technique captures all such events (as shown by red atoms which do not have perfect FCC lattice structure). Finally, it is observed that CNA technique studied in the present paper is a much simpler and easier way to track the crack tip location for a growing crack. The growing crack tip location may be identified accurately by tracking the CNA patterns along the length of the crack.

4. Prediction of stable crack growth and corresponding crack speed

During a uniaxial tensile loading (for a pre-cracked sample), it is important to know that whether the crack under investigation is stable or not at a particular load step (under displacement controlled loading) before applying any further loading. The stability of the crack/ crack growth would lead to the identification of accurate crack growth rate (i.e., the crack speeds). Hence, the relaxation period between two consecutive load steps is an important parameter for studying the stability of crack growth and for accurate crack growth rate prediction. In the recent past, many attempts have been made to identify crack growth rate of single crystal utilizing molecular dynamics simulations. For example, an average crack speeds during various stages of crack growth of single crystal Al is shown in [25]. An increase in average crack speed is reported with an increase in crack length, for example during initial crack blunting an average crack speed of 146.7 m/s, during initial crack growth and at first void nucleation an average crack speed of 768 m/s, during second void nucleation an average crack speed of 1497 m/s, and during third void nucleation an average crack speed of 2318 m/s, are reported. A constant rate of loading at the top boundary of the structure is applied without any relaxation time between two consecutive loading steps in Xu and Deng (2008). However, it is not clearly demonstrated in Xu and Deng (2008) that whether the growing crack is reached its maximum limits (crack is stable or not) before the application of next load step.

In another study, an incremental displacement loading during MD simulations of Al single crystal for the prediction of stress behavior and traction-separation law is used (Krull and Yuan 2011). A relaxation period of 25ps is considered between two consecutive loading steps. However, no attempts have been made to calculate crack growth as well as crack speed (Krull and Yuan 2011). Also, it is not shown that whether the relaxation period of 25ps considered between two loading step will have any impact on the results presented in Krull and Yuan (2011). Krull and Yuan (2011) have also demonstrated various events during the crack initiations and crack growth. It is also important to mention here that the first events of crack growth (for example, crack tip blunting, initial crack growth, void nucleation, void growth and coalescence etc.) have also been identified in Krull and Yuan (2011). The corresponding structural configurations are considered for the post processing of various stress behaviors including tensile stress, hydrostatic stress, Von-Mises stress. However, the stability of the crack growth is not been considered for studying various stress behaviors (Krull and Yuan 2011). In an another study (Wu and Yao 2012), a relaxation time of 20ps is considered while performing MD simulation of Ni single crystal to find out the crack growth and stress behavior with varying temperature. The crack length is calculated every 1ps for a total of run time 600ps in Wu and Yao (2012) without discussing the fact of the

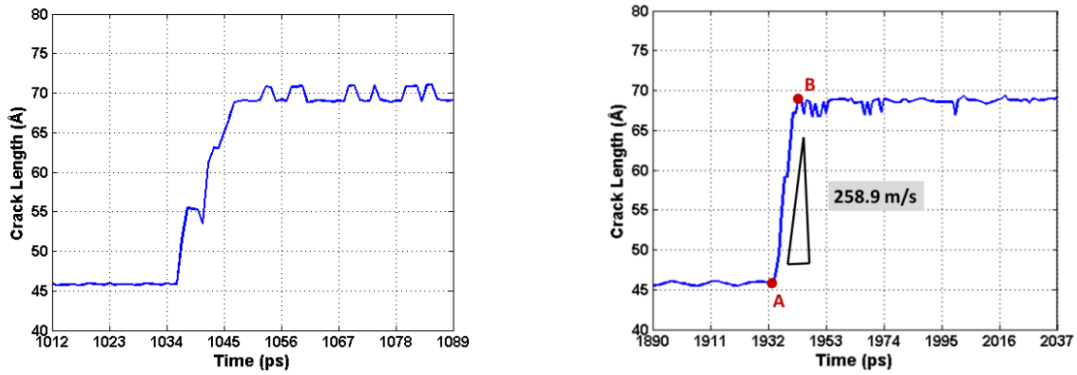

(a) (b)

Fig. 5 Crack length v/s Time (ps) plot for CNA approach for predicting crack growth with varying relaxation time of (a) 10ps and (b) 20ps considered between two consecutive displacement controlled loadings. (Each block consists of 1ps of displacement controlled loading step and then subsequent 10 or 20ps of relaxation periods. For example, figure 5(a) shows scale of 1012 to 1023, in which 1012-1013 periods consist of displacement controlled loading step of 1ps and 1013-1023 periods consist of 10ps of relaxation step. Similarly, figure 5(b) shows scale of 1911 to 1932, in which 1911-1912 periods consist of displacement controlled loading step of 1ps and 1912-1932 periods consist of 10ps of relaxation step.)

stability of the growing crack. Results are compared with varying temperature and interpretations are made as temperature being considered as a key parameter on the prediction of crack growth. It is possible that the interpreted results may lead to totally different conclusions if the stability of crack growth is not considered for the identification of crack length.

In this direction, firstly, stability of crack growth is demonstrated and it is shown that how the relaxation time leads to different crack growth behaviors. Next, crack speed is calculated based of stable crack growth region and the relaxation time. Finally, an efficient and simple method of varying relaxation time is proposed for predicting crack growth length.

In order to demonstrate the effect of relaxation time on the crack growth and crack speed, six different cases are considered. First case is similar to what is used in Xu and Deng (2008) where a constant rate of loading at the top boundary of the structure is applied without any relaxation time between two consecutive loading steps. Other five cases are in which the relaxation time of 10ps, 20ps, 30ps, 40ps, 50ps are considered between two consecutive displacements controlled loading steps (refer section 2.2 for further details on loading). These procedures are similar to what is used in (Krull and Yuan 2011, Wu and Yao 2012), where the relaxation time of 25ps and 20ps are considered, respectively.

Fig. 5 shows the variations of crack length with time for two different relaxation periods shown here for demonstration. The relaxation period of 10ps and 20ps are considered in Figs. 5(a) and (b), respectively. The displacement controlled loading is applied in 1ps and then the system is equilibrated for the corresponding relaxation time before the application of the next loading. Each grid box of Fig. 5(a) is consist of 11ps that includes 1ps (i.e., 1012-1013 in Fig. 5(a)) of displacement controlled loading and remaining 10ps (i.e., 1013-1023 in Fig. 5(a)) of relaxation time. It can be seen that no crack growth has been seen (as there is no increase in crack length in the time interval of 1012-1023ps and in the time interval of 1023-1034ps); hence, the crack is

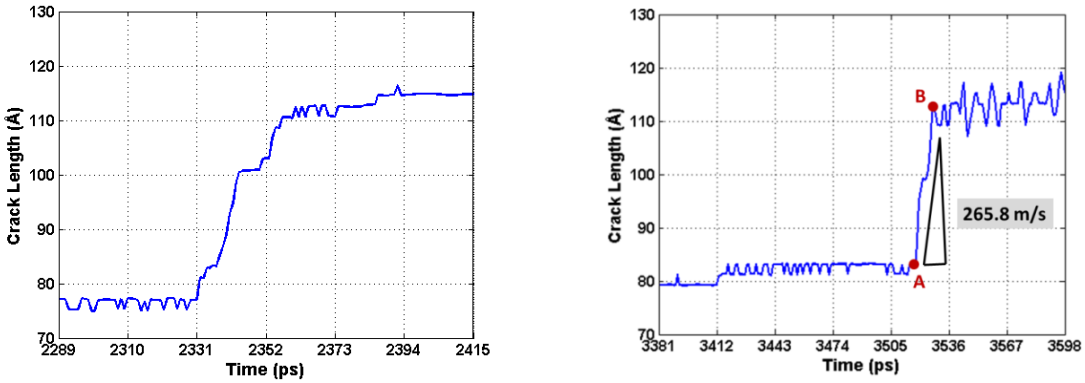

(a) (b)

Fig. 6 Crack length v/s Time (ps) plot for CNA approach for predicting crack growth with varying relaxation time of (a) 20ps and (b) 30ps considered between two consecutive displacement controlled loadings

stable as the crack is reached to its maximum crack growth limit in that particular loading step. However, in the time interval of 1034-1045ps, it can be seen that the crack is keep on growing and did not reach to a constant crack length in a given relaxation time period; hence, it indicates that 10ps of relaxation time is not sufficient for the crack to get stable in that particular loading step of 1034-1045ps. Hence, the application of the next step of displacement loading in the time interval of 1045-1056ps may suppressed the crack growth behavior of previous step. The time interval of 1034-1045ps indicates that at this stage of loading a larger relaxation time is required for crack to grow completely and to reach a stable state. Hence, an increased relaxation time of 20ps is considered next, as shown in the Fig. 5(b). It can be seen in the Fig. 5(b) that initially the crack is stable for the time interval 1890-1911ps and 1911-1932ps. Later, the crack started growing in the time interval of 1932-1953ps, however, it can be seen that the crack has reach its stable limit (i.e., maximum crack length limit) in this particular time interval. In the cases, where the crack growth has reached a stable condition, the crack speed is calculated, as shown in Fig. 5(b). The time interval of 1932-1953ps where a stable crack growth is seen shows a crack speed of ~258.9m/s. Above studies indicate that the 20ps of relaxation time is required for the crack to reach stable configuration in this particular step of loading.

On the other hand, if we look closely to the time interval between 1890-1911ps (refer Fig. 5 (b)), it can be seen that 10ps of relaxation time could have been sufficient for the crack to reach stable state as no crack growth is seen in that loading step. Hence, using a larger relaxation time of 20ps between two consecutive displacements controlled loadings in the time interval between 1890-1911ps is computationally more costly. It also indicates that utilization of a constant relaxation time may lead to higher computation cost for the same results. In order to reduce the computation cost for predicting crack growth, a variable relaxation time based algorithm is proposed, as discussed in the subsequent section.

The relaxation time period of 30ps, 40ps, and 50ps is also considered in the present study as it is observed that with further increase of crack length the relaxation time of 20ps is found not to be sufficient for obtaining a stable crack. This is demonstrated in Fig. 6. Figs. 6 (a) and (b) is corresponding to 20ps and 30ps of relaxation time between two consecutive loading steps. The

Table 1 Algorithm for the calculation of stress and traction-separation data

Step 1	Apply displacement controlled loading for 1ps
Step 2	Equilibrate structures for minimum 10ps and check last 5ps data (last 5 data point needs be checked whether the crack is become stable or not) if yes go to Step 3 else equilibrate till last 5ps data becomes constant
Step 3	Average out the last 5ps data
Step 4	Compute and store stress data and traction-separation data
Step 5	Go to Step 1

time interval of 2331-2352 (20ps relaxation time) shows that crack is not reached its stable state (as the crack length is increasing linearly with time from ~80Å to ~110Å) before the next increment of displacement controlled loading. Hence, a further increase in relaxation time is required to obtain a stable crack length, as shown in Fig. 6(b) with a 30ps relaxation time. It can be seen from the Fig. 6(b) that the crack length reached a stable state during the 30ps relaxation time (as can be seen that crack grows from ~80Å to ~110Å during time interval of 3505-3536ps). The crack speed for a stable growth of crack in this region has also been calculated, as shown in Fig. 6(b). The time interval of 3505-3536ps where a stable crack growth is seen shows a crack speed of ~265.8m/s. The calculation of crack speed indicates that during the stable crack growth the crack grows with a speed lower that the speed of sound (330m/s). Above results indicate that <100> oriented Al shows almost a constant crack speed during the stable crack growth process.

In order to reduce the computation times without compromising the results, a simple and robust algorithm is proposed here that utilizes a variable relaxation time period for the computation of crack growth, (also for stress behavior and traction-separation atomistic law). In the proposed algorithm, an initial displacement controlled loading is applied at step 1. Later, the atomistic configuration considered during study is initially equilibrated for 10ps at step 2. The data of last 5ps is analyzed for checking the crack growth stability. The last 5 data points of 5ps are evaluated and it is checked whether the crack growth is constant in the last 5 data sets or not. If the crack is found to be still growing in the last 5 data sets, the system configuration is further allowed to equilibrate (in subsequent steps of 5ps) before application of next loading step. This process will continued till the last 5ps data is observed constant for a given load step. Once the stable crack is achieved, the last 5ps data is averaged for the computation of traction-separation law in the step 3 (a detailed discussion on the effect of crack stability on the traction - separation law is presented in section 6). In the step 4, the computation of stresses and traction-separation data is performed and stored. Next, subsequent displacement controlled loading is applied in the step 5 and it continues till the complete data is generated.

5. Stress behavior during crack initiation and crack growth

In this section, a detailed study of various stress quantities is explored including tensile stress, Von-Mises stress, and hydrostatic stress. This section is further divided into two parts: (1) event based stress behavior and (2) stable region based stress behavior. In the event based stress behavior, firstly, various events have been identified from the post processed data via visualizing the structure as done in Krull and Yuan (2011), Xu and Deng (2008). This process includes initial crack tip, crack tip blunting, crack initiation and growth, void nucleation, void growth and

coalescence process. Once the events are identified from the post processed data, the corresponding stress data has been considered for the visualization of various stress patterns as well as averaged stress behavior along the crack length axis, as shown in Fig. 7. On the other hand, in the second method, stresses are visualized based on stability criteria of crack. Firstly, the stable regions are identified from the crack length versus time plots (see Figs. 3 and 4 for further details) and the corresponding time step has been considered for the visualization of various stress patterns as well as averaged stress behavior along the crack length axis, as shown in Fig. 8.

5.1 Event based stress behavior

Identification of events during the crack initiation and growth of the single FCC crystal simulations consist of four major stages, i.e., (1) crack tip blunting, (2) crack growth initiation, (3) void nucleation and growth, and (4) void coalescence and crack growth. The similar phenomena of event based crack initiation and crack growth has already been demonstrated in Krull and Yuan (2011), Xu and Deng (2008).

When the crystal is stretched by the displacement loading, a stress concentration develops at the crack tip due to geometric discontinuity. As loading continues, the intensity of stress concentration at the crack tip builds up and atoms at the crack tip move apart in such a way as to expand the size of the crack tip, leading to severe local straining at the crack tip and eventually to crack tip blunting when the stress intensity reaches a certain critical level. To illustrate the above observation, Fig. 7 shows the field contours of the tensile stress (snapshot (i) of Figs. 7(a) and (b)), the hydrostatic stress (snapshot (ii) of Figs. 7(a) and (b)), and the Von-Mises stress (snapshot (iii) of Figs. 7(a) and (b)) around the crack tip just before (at 1937 ps) and after (at 1948 ps) crack tip blunting. To provide a more quantitative understanding of the stress field just before and after crack tip blunting, the variations of the three stress quantities along the crack line with the distance to the crack tip are plotted in snapshot (iv) of Figs. 7(a) and (b). At the time of t=1937ps after loading is initiated, as shown by the contour levels in snapshots (ii) and (iii) of Fig. 7(a) and by the field variations in the snapshot (iv) of Fig. 7(a) ahead of the crack tip along the crack line, the Von- Mises stress and the hydrostatic stress both have their highest values at the crack tip.

A close examination reveals that the blunting of the crack tip is actually accompanied by a small amount of crack extension, which can be considered as the onset of initial crack growth. This observation can be made from comparing the crack tip location in snapshot (i) of Figs. 7 (b) and (c). After the onset of crack growth, the initial period of crack growth continues as the remote displacement loading continues. During this initial crack growth process, the overall field contour patterns for the tensile stress, the Von-Mises stress, and the hydrostatic stress around the moving crack tip remain similar, that is, the near-tip field patterns move with the crack tip in a self-similar manner (for example, compare snapshot (iii) of Figs. 7(b), (c), and (d)).

The initial period of crack growth after crack tip blunting does not last long before the crack growth process is filled with events involving void nucleation and growth at a short distance ahead of the crack tip. At t=2410ps (just before the emergence of the first void) the intensity of concentration (see Fig. 7 (d)) of the hydrostatic stress has reached its highest levels since the onset of crack growth. It can also be seen from the snapshot (iv) of Fig. 7 (d) that a small dip in the stress at the vicinity of voids (between the initial crack tip and the present crack tip). The dip is observed in all the three stresses, i.e., the tensile stress, the Von-Mises stress, and the hydrostatic stress.

At t=2462ps (just before the nucleation of the second void), the stress contours (Fig. 7(e))

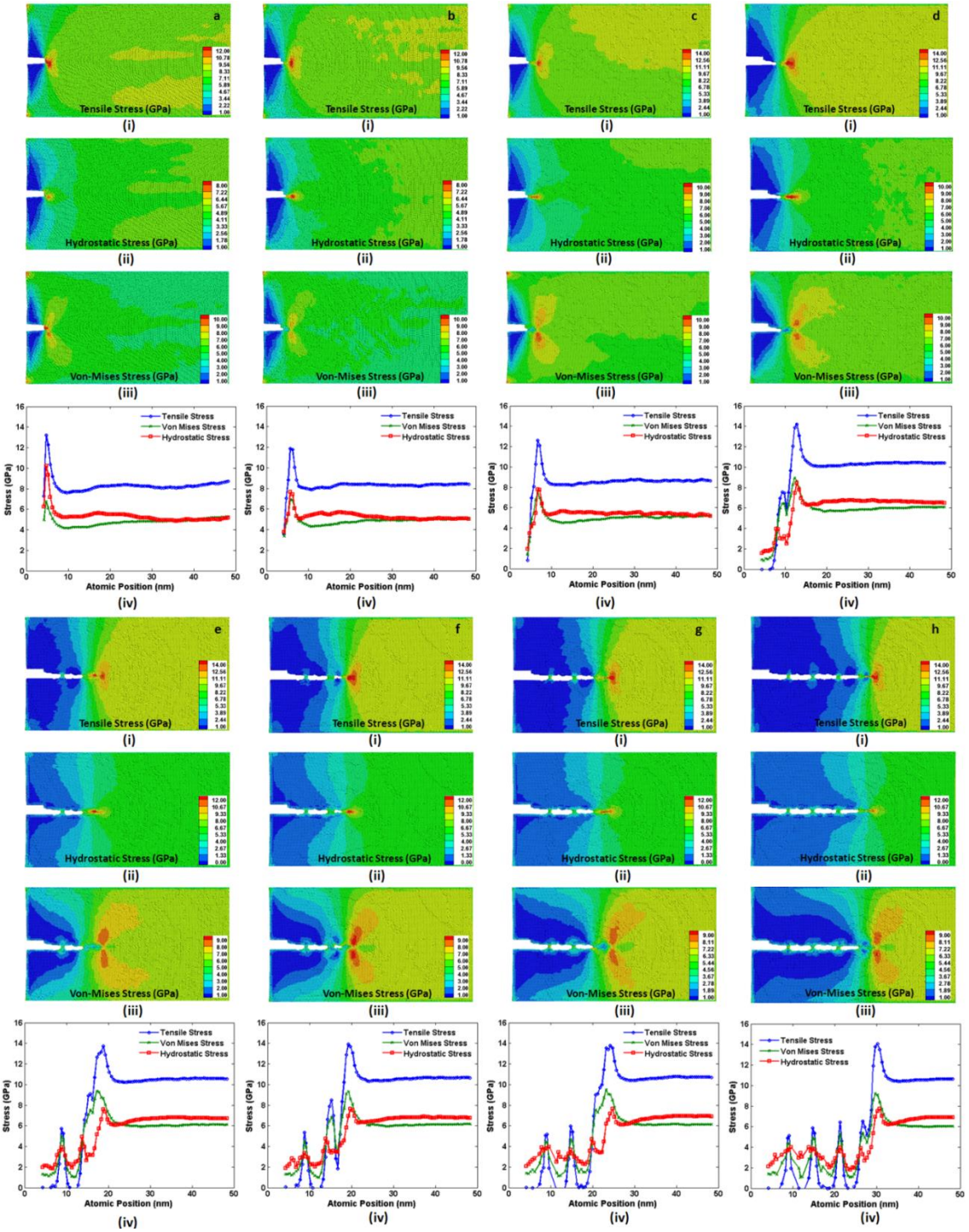

Fig. 7 (a) Just before crack tip blunting (1937ps), (b) after crack tip blunting (1948ps), (c) during initial crack growth (2289ps), (d) before first void nucleation (2410ps), (e) just before second void initiation (2462ps), (f) during second void growth (2469ps), (g) during third void initiation (2482ps), and (h) after fourth void initiations (2496ps)

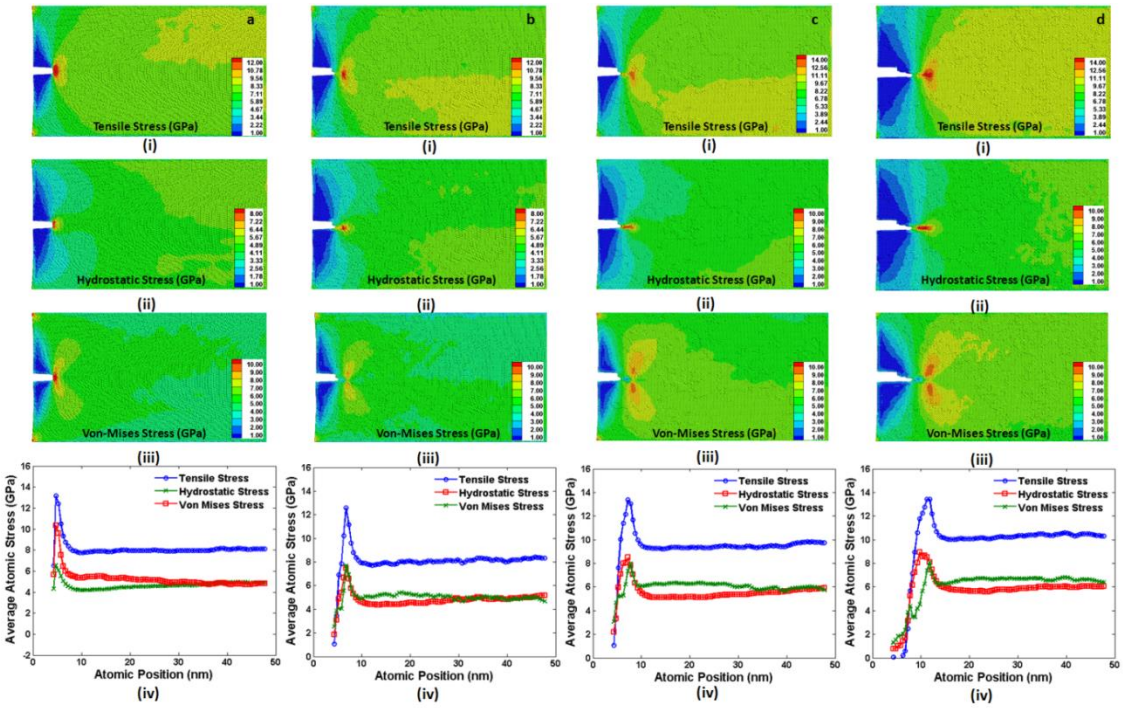

Fig. 8 (a) Just before crack tip blunting (1934ps), (b) after crack tip blunting (1950ps), (c) during initial crack growth (2286ps), and (d) during further crack growth (2414ps)

continue to show a concentration of the hydrostatic stress and the Von-Mises stress ahead of the first void. Further loading leads to the formation of a ligament, as can be seen in Fig. 7(e). The corresponding peak in stress along the crack length axis can also be seen in snapshot (iv) of Fig. 7(e). This process shows the void growth and coalescence. At t=2469ps shows the formation of second voids as can be seen in Fig. 7(f). Simulation results strongly suggest that the process of void nucleation and void growth will repeat itself as the remote displacement loading increases. That is, as loading continues, a new void will be nucleated ahead of the forward tip of the leading void. To this end, it is noted that in the MD simulation of the current study a third and fourth void is indeed nucleated at the expected location shortly after t=2482ps and 2496ps, as shown in Figs. 7(g) and (h), respectively.

5.2 Stable region based stress behavior

In this section, identification of events during the crack initiation and growth of the single FCC Al crystal simulations are obtained based on the stable region data (as demonstrated in the section 4). The stable region of crack initiation and growth consist of the following steps: (1) crack tip blunting, (2) crack initiation, and (3) crack growth.

Figs. 8(a) and (b) shows the sample just before and after the crack tip blunting at t=1934ps and 1950ps, respectively. A similar stress behavior (as demonstrated in the section 5.1) along the crack length axis is seen. A close examination reveals that the blunting of the crack tip is actually accompanied by a small amount of crack extension, which can be considered as the onset of initial

crack growth. This observation can be made from comparing the crack tip location in snapshot (i) of Figs. 8(a) and (b). It can also be seen from the snapshot (iv) of Figs. 8(b) that a small dip in the Von-Mises stress is observed in the stress plot. This indicates that the crack growth process is filled with events involving void nucleation and growth at a short distance ahead of the crack tip. It is important to mention here that the process of void nucleation and its growth has been observed during the process of relaxation of the structure; hence, indicating that the void nucleation and the corresponding void growth are the phenomena observed during the unstable crack growth process.

At t=2286ps the crack further grows and the shifting of the maximum value of stress can be seen ahead of new position of crack tip, as shown in Fig. 8(c). It is again seen here that the Von-Mises stress is able to capture the voids details, as a small dip (position between the initial crack tip and the present crack tip) in the stress plot can be seen in the snapshot (iv) of Fig. 8(c). Further loading leads to more void nucleation and grow (occurs during the unstable crack growth process) that finally leads to the growth of crack, as can be seen in Fig. 8(d). It is also important to mention here that no ligaments have been formed during the stable crack growth process. Hence, it can be concluded that the stable region data only consist of crack tip blunting, crack initiation, and crack growth; however, the void nucleation, void coalescence, and crack growth (observed intermediately during the relaxation period) are the phenomenon observed during the unstable crack growth process.

6. Identification of traction-separation law

Three different approaches are explored in this paper for the calculation of traction-separation law from the atomistic simulations data. These are: (1) continuous data at equal intervals, (2) stable region data only, and (3) CNA independent Stable region Data.

6.1 Continuous data at equal intervals

In this method, a similar technique as proposed in Krull and Yuan (2011) is used. Krull and Yuan (2011) have used every 5ps data (from the time interval of 0-315ps) for the calculation of atomic cohesive law. In the present paper, data at every 10ps data is used (due to the large set of data used as compared to Krull and Yuan (2011)) for the calculation of atomic cohesive law from the time interval of 0-2500ps. First, we will discuss the data presented in Krull and Yuan (2011) and the interpretation made on the traction separation law. Later, the results generated during the present work will be discussed.

It is reported in Krull and Yuan (2011) that if the separation becomes larger near the vicinity of crack tip, damage occurs in the material. It is indicated by the typically non-linear decreasing of the traction-separation curve in Krull and Yuan (2011). The reported curve shows a wide scatter band in the region beyond the elastic deformations, since the data contained traction and separation in all stages (i.e., near the crack tip region, ahead of crack tip region, and further ahead near the boundary region) of atoms along the crack path. It is also indicated in Krull and Yuan (2011) that the stress state for crack initiation has to be different from the steady-state crack growth, so that the traction-separation relations for these two events have to be different. In order to analyze this scatter band, the cohesive zone region was divided into three vertical regions: (1) Region up to 4.5 nm ahead of the initial crack tip, where the initial crack growth happens. (2) Region of void nucleation, growth and coalescence, which is between 4.5 nm and 24.0 nm ahead of the initial

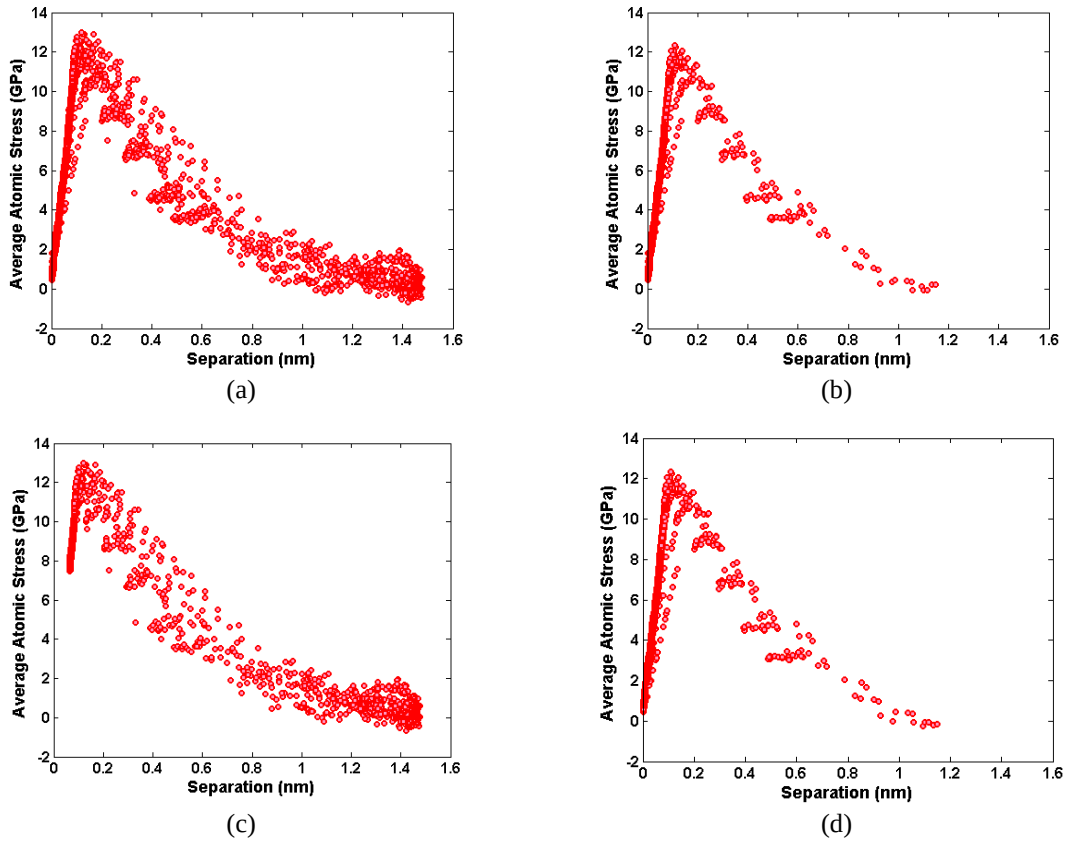

Fig. 9 Traction-separation data for different methods (a) Method - 1 (i.e., continuous data in equal intervals of 10ps), (b) Method - 2 (i.e., stable region data only), (c) removal of stable region data from Method -1, and (d) Method - 3 (i.e., CNA independent stable region data)

crack tip. (3) Region greater than 24.0 nm ahead of the initial crack tip, where the deformation is purely elastic in the present computations (see Fig. 5 of Krull and Yuan (2011) for further details). It is also shown that the third region is dominated by the elastic deformation, because the crack does not run into this part of the cohesive zone.

Fig. 9 (a) shows the traction-separation data generated in the present work using the above procedure (as discussed in Krull and Yuan (2011)) with a step of 10ps and a time interval of 0-2500ps. It can be seen that the trends of total traction-separation atomistic law generated in Krull and Yuan (2011) (refer Fig. 5(a) of Krull and Yuan (2011)) is similar to what is shown here in Fig. 9 (a). It is shown in Krull and Yuan (2011) that at first region (i.e., region up to 4.5 nm ahead of the initial crack tip, where the initial crack growth happens) during initial crack growth the scatter band in the cohesive law are very large since the failure process for that region is constant. Hence, it is concluded that the initial crack starts to grow at different maximum tractions and is not in a steady-state. However, no attempt has been made to see that whether the crack growth considered is in steady-state or not. Also, it is important to mention here that the region 1 (cell 1 to 11) considered in Krull and Yuan (2011) is not only contribute for the initial crack initiation, however, the region will also contributes during the void nucleation, void growth and coalescence process.

However, it is also mentioned in Krull and Yuan (2011) that more detailed computations are necessary to figure out the inter-dependence among crack initiation, void nucleation, and traction. In this direction, an in-depth study of inter dependency of crack initiations, void nucleation, and traction are performed in this section.

It is also shown in Krull and Yuan (2011) that in the second region (cell 12 to 64) the scatter band becomes narrow and a clear trend of the cohesive law is visible. Hence, it is hypothesized that the discrete failure process approached as a continuous crack growth, which becomes steady and the data of this region is considered for the calculation of traction-separation atomistic law. However, it is important to mention here that the second region data (between 4.5 nm and 24.0 nm ahead of the initial crack tip) that will also be the part of initial crack tip blunting and crack initiations as the crack progress further. Hence, the selection of traction-separation law based on particular region is not justifiable. In this direction, a schematic study is performed in the present paper to understand the various mechanisms that leads to the scattering in traction - separation data. Also, a more accurate procedure for the generation of traction-separation atomistic law is proposed in this paper in the subsequent section.

6.2 Stable region data only

In this section, a new scheme for the accurate prediction of cohesive law is proposed. Only stable region of crack growth data and the corresponding time step is considered for the calculation of atomic cohesive law instead of continuous 10ps of time interval of data as done in the previous section. The calculation procedure of stable crack growth calculation is shown in Table 1. The corresponding traction-separation atomistic data is shown in Fig. 9 (b). It can be seen that the data is smoother as compared to the method discussed in section 6.1. It is important to mentioned here that the stable region of crack growth data consist of only the crack tip blunting, crack initiations, and crack growth without any formation of void nucleation, void growth, and coalescence process. It is already discussed that the formation of void nucleation, void growth, and coalescence process is observed only in the unstable crack growth region. It could be interpreted from the results the scattered in the Fig. 9 (a) is mainly because of the unstable crack growth and it consists of void nucleation, void growth, and coalescence process. This is also confirmed by removing the data points of stable region (data used for generate Fig. 9(b)) from the Fig. 9 (a) and plotted separately in Fig. 9 (c), which is mainly because of void nucleation, void growth, and coalescence process. It can be seen in Fig. 9 (c) that the scatter band in the cohesive law is very large. Hence, it is concluded here that the void nucleation, void growth, and coalescence process starts to grow at different maximum tractions and is not in a steady-state.

6.3 CNA independent stable region data

In this section, another scheme is proposed for studying scattering of raw atomistic data. In this method, an atom who's CNA is not equal to the bulk FCC is neglected while performing the averaging of stress (refer Fig. 2 for further details). This is done due to the fact that the atoms at the surfaces are found to be having higher stresses as compared to the bulk counterpart and it may cause fluctuations of data during the generation of cohesive law. The stable region data is with CNA $\neq 5$ is considered in this method while performing averaging of stresses over a given region. The calculated traction-separation data is shown in Fig. 9(d). It is observed that the pattern is similar to Method -2 (refer section 6.2) as shown in Fig. 9(b). It is observed that this method does

not lead to any further improvement over Method - 2. Hence, the prediction of traction-separation data utilizing stable crack region data (Method - 2) is considered for the next set of studies (performed in the 6.1, 6.2, and 6.3) the atoms near the crack tip are considered while formulation of process zone for the prediction of crack growth or traction-separation law and also in (Krull and Yuan 2011, Wu and Yao 2012, Xu and Deng 2008). In order to find out the effect of atoms at the free surface of initial crack tip on the generation of traction-separation atomistic law, another study is performed, as discussed later in section 8.

7. Empirical curve-fitting for traction-separation law

In this section, the polynomial potential utilized for describing the process of void nucleation from initial debonding through complete decohesion, as proposed in Needleman (1987) for bulk material has been used for comparing the MD results obtained in the present study. Also, the popular form of exponential potential (Needleman 1990) which is utilized for interface modeling and for analyzing the initiation and development of decohesion along interfaces in bulk materials in recent past has also been compared. The polynomial form of the potential ($\emptyset$) used here that represents the mechanical response of the interface and can be described through a constitutive relation that gives the dependence of the tractions T_n (opening, Mode - I), T_t (shear, Mode - II), and T_b (tearing, Mode - III) on separations $u_n, u_t,$ and u_b as (Needleman 1987)

$$\emptyset\left(\mathrm{u_n},\mathrm{u_t},\mathrm{u_b}\right)=\frac{27}{4}\sigma_{\max}\delta\left\{\begin{array}{l}\frac{1}{2}\left(\frac{\mathrm{u_n}}{\delta}\right)^2\left[1-\frac{4}{3}\left(\frac{\mathrm{u_n}}{\delta}\right)+\frac{1}{2}\left(\frac{\mathrm{u_n}}{\delta}\right)^2\right]+\\ \frac{1}{2}\alpha\left(\frac{\mathrm{u_t}}{\delta}\right)^2\left[1-2\left(\frac{\mathrm{u_n}}{\delta}\right)+\left(\frac{\mathrm{u_n}}{\delta}\right)^2\right]+\\ \frac{1}{2}\alpha\left(\frac{\mathrm{u_b}}{\delta}\right)^2\left[1-2\left(\frac{\mathrm{u_n}}{\delta}\right)+\left(\frac{\mathrm{u_n}}{\delta}\right)^2\right]\end{array}\right\} \tag{7}$$

where $\sigma_{\max}$ is the maximum traction carried by the interface undergoing a purely normal separation ($u_t \equiv u_b \equiv 0$), δ is a characteristic length, and α specifies the ratio of shear to normal stiffness of the interface. The interfacial tractions are obtained by differentiating Eq. (7). The normal component of traction $T_n = -\frac{\partial \emptyset}{\partial \mathrm{u_n}}$ considered in the present context is as

$$\mathrm{T_n}=\frac{-27}{4}\sigma_{\max}\left\{\begin{array}{c}\left(\frac{\mathrm{u_n}}{\delta}\right)\left[1-2\left(\frac{\mathrm{u_n}}{\delta}\right)+\left(\frac{\mathrm{u_n}}{\delta}\right)^2\right]+\\ \alpha\left(\frac{\mathrm{u_t}}{\delta}\right)^2\left[\left(\frac{\mathrm{u_n}}{\delta}\right)-1\right]+\\ \alpha\left(\frac{\mathrm{u_b}}{\delta}\right)^2\left[\left(\frac{\mathrm{u_n}}{\delta}\right)-1\right]\end{array}\right\} \tag{8}$$

It is assumed that the interface undergoing a purely normal separation ($u_t \equiv u_b \equiv 0$). This assumption could be made in the present context due to the periodic boundary conditions considered at out of plane loading directions. Hence, the Eq. (8) can further be simplified as

$$\mathrm{T_n}=\frac{-27}{4}\sigma_{\max}\left\{\left(\frac{\mathrm{u_n}}{\delta}\right)\left[1-2\left(\frac{\mathrm{u_n}}{\delta}\right)+\left(\frac{\mathrm{u_n}}{\delta}\right)^2\right]\right\} \tag{9}$$

The polynomial form of traction as shown in Eq. (9) is used in the present paper for fitting of MD results. On the other hand, the exponential form of potential ($\emptyset$) can be written as (Needleman

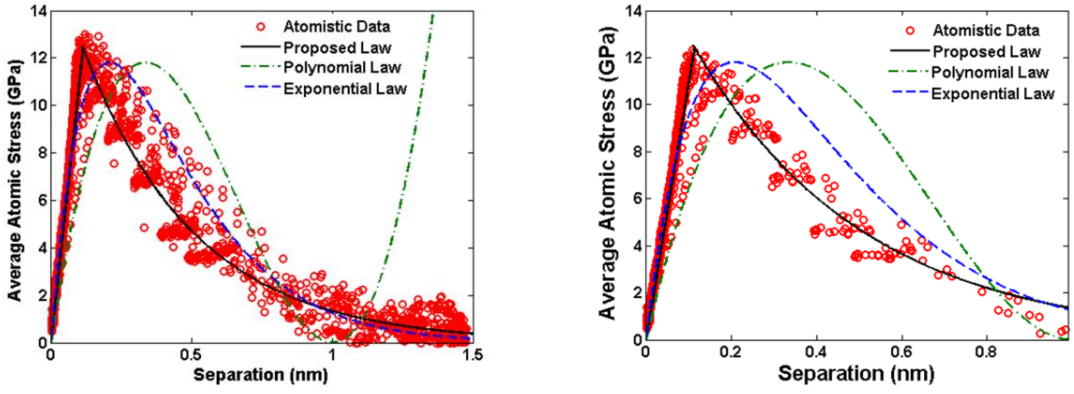

Fig. 10 Traction-separation data for different methods (a) Method - 1 (i.e., continuous data in equal intervals of 10ps), (b) Method - 2 (i.e., stable region data only). The Polynomial law of Needleman (1987), Exponential law of Needleman (1990), and the law proposed in the present paper are also plotted

1990)

$$\emptyset\,(u_n, u_t, u_b) = \frac{9}{16}\sigma_{max}\delta\left\{1 - \left[1 + z\left(\frac{u_n}{\delta}\right) - \frac{1}{2}\alpha z^2\left(\frac{u_t}{\delta}\right)^2 - \frac{1}{2}\alpha z^2\left(\frac{u_b}{\delta}\right)^2\right]\exp\left[-z\left(\frac{u_n}{\delta}\right)\right]\right\} \quad (10)$$

$z = \frac{16e}{9}$, with $e = \exp(1)$. The normal component of traction $T_n = -\frac{\partial \emptyset}{\partial u_n}$ considered in the present context is as

$$T_n = -\sigma_{max} e\left\{z\left(\frac{u_n}{\delta}\right) - \frac{1}{2}\alpha z^2\left(\frac{u_t}{\delta}\right)^2 - \frac{1}{2}\alpha z^2\left(\frac{u_b}{\delta}\right)^2\right\}\exp\left[-z\left(\frac{u_n}{\delta}\right)\right] \quad (11)$$

It is assumed that the interface undergoing a purely normal separation ($u_t \equiv u_b \equiv 0$). Hence, the Eq. (11) can further be simplified as

$$T_n = -\sigma_{max} e z\left(\frac{u_n}{\delta}\right)\exp\left[-z\left(\frac{u_n}{\delta}\right)\right] \quad (12)$$

The exponential form of traction as shown in Eq. (12) is also used in the present study for fitting of MD results. The similar form of exponential traction law is also used in Krull and Yuan (2011) for fitting their MD data. In the present paper, the value of $\sigma_{max} = 11.96$ GPa and the critical value of separation of $\delta = 1.0$ is considered.

It can be seen from the Fig. 10 (a) that the polynomial form of fitting does not give an accurate representation of data based on the above considered fitting parameters. On the other hand, the exponential form of fitting provides a more realistic behavior of MD data. However, the peak of the initial traction-separation region (also the initial linear region of Figs. 9 and 10) is not able to capture by the exponential form. Also, the region next to the maximum traction towards the critical separation, the fitting provides a good correlation only for the full region of data. However, the stable region of data as shown in Fig. 10(b) does not provide a good exponential fitting. In order to capture the initial region accurately up to the maximum traction, a modified fitting law is proposed in the present paper. The proposed law consists of two parts, the first part shows linear behavior and the second part shows the exponential behavior as

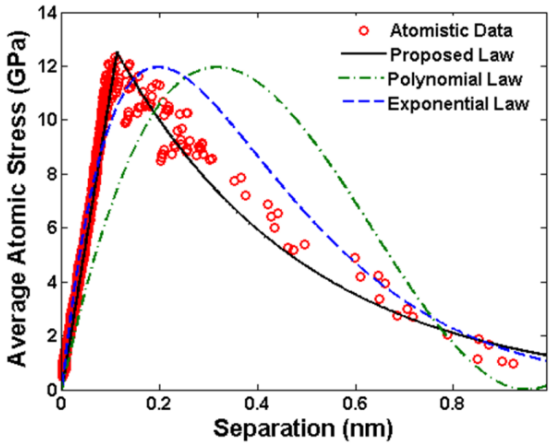

Fig. 11 Traction-separation data for Method - 2 (i.e., stable region data only) to study the effect of surface stress. The Polynomial law of Needleman (1987), Exponential law of Needleman (1990), and the law proposed in the present paper are also plotted

$$T_n = \sigma_{max}\left(\frac{u_n}{\delta}\right) \qquad \text{for } 0 \le \delta \le u_n|_{\sigma_{max}} \tag{13a}$$

$$= \sigma_{max}\, A \exp\left[-2A\left(\frac{u_n}{\delta}\right)\right] \qquad \text{for } \delta \ge u_n|_{\sigma_{max}} \tag{13b}$$

where the fitting parameters of $A = \frac{7}{5}$ and $u_n|_{\sigma_{max}} = 0.1078$ nm is considered. The remaining values of maximum traction and critical separation considered are similar to what is discussed above. It can be seen from the Figs. 10(a) and (b) that the proposed traction-separation law gives more accurate prediction for <100> oriented FCC Al single crystal. However, a detailed study of other orientations on the proposed traction-separation law and on the other FCC materials is still an open area of research. It is important here to mentioned that the polynomial (Needleman 1987) and exponential (Needleman 1990) model considered here to fit the atomistic data, used previously for generation of cohesive law for bulk materials. However, an attempt has been made in the present study to understand the effect of polynomial ad exponential model on the nano-scale behavior.

8. Surface effects on the traction-separation law

A small clutter of data in the initial linear region of traction-separation data can be seen during stable crack growth region as shown in the Fig. 9(b). In the above study as well as the studies performed in (Krull and Yuan 2011, Wu and Yao 2012, Xu and Deng 2008), region starting from the crack tip is considered for the generation of traction-separation data (for example see Fig. 2 of Krull and Yuan (2011)). It is well known that the free surfaces near the crack tip have higher stresses as compared to the bulk counterpart of the structure. The stresses at the free surface at the crack tip may affect the traction-separation law and also could be the reason for the fluctuation in

the traction-separation data shown in the Fig. 9 (b). In order to investigate the effect of surface effects, a modified region (without consideration of small strip of atoms ahead of initial crack tip) is considered with stable crack growth regions only, as shown in Fig. 2 (b). The atoms with twice the cut-off radius are neglected near the crack tip for the calculation of traction-separation law for a stable crack growth region. The calculated traction-separation law with modified region (neglecting the surface atoms at the crack tip) is shown in Fig. 11. It can be seen that the fluctuations in the data of Fig. 9 (b) in the vicinity of linear region of curve is suppressed. Results indicate that the fluctuations in the traction-separation data could be controlled by proper selection of regions (avoiding any surface effects as well as boundary regions) during the cohesive law computations. However, the effects of surface as well boundary regions on the traction - separation law could be implemented into the proposed law that requires further studies of different crack surface as well as boundary conditions. The proposed traction-separation law (Eq. (13)) is also plotted in the Fig. 11 along with the polynomial (Needleman 1987), and exponential law (Needleman 1990) proposed for bulk materials. The proposed law gives an excellent fit as compared to the polynomial and exponential law.

9. Conclusions

A simpler and easier approach of CNA for the accurate prediction of crack growth is proposed. It is also demonstrated that CNA approach is more accurate as compared to the threshold potential energy approach at ~0K; however, the effect of temperature needs elaborate studies. Next, a procedure of prediction of crack speed is demonstrated based on the stable crack growth criteria. A simple and robust algorithm is also proposed that utilizes a variable relaxation time period for the computation of crack growth, stress behavior, and traction-separation atomistic law. A detailed study of stress behavior near the vicinity of crack tip is performed. Pattern of averaged tensile stress, averaged hydrostatic stress, and averaged Von-Mises stress are studied. It is found out that the averaged Von-Mises stress is able to capture the details of void nucleation during the stable crack growth process. It is also demonstrated that the newly proposed scheme, i.e., based on the time interval of stable region of crack leads to a smoother traction-separation law. The traction-separation data obtained via MD is also fitted with the existing polynomial and exponential law utilized for bulk materials. It is found that both the polynomial and exponential law is not able to predict the traction-separation law accurately. A new curve fit is proposed in the paper that predicts accurately the traction-separation data generated by MD. Effect of surface atoms and there corresponding effects on the overall traction-separation law is also studied. Result shows that the surface atom near the crack tip lead to the more scatter in the traction-separation law, however, a further detailed study with different orientations and crack surface is still an open area of research.

Acknowledgements

NS and DRM thankfully acknowledge the use of computational facilities at the ACECOST Computational Science Lab, Department of Aerospace Engineering, IISc and funding under ACECOST Phase-III program of Aeronautics Research and Development Board, India.

References

Abraham, F.F. and Broughton, J.Q. (1998), "Large-scale simulations of brittle and ductile failure in fcc crystals", *Comput. Mater. Sci*., **10**, 1-9.

Amarillas, A.P. and Garzón, I.L. (1996), "Microstructural analysis of simulated liquid and amorphous Ni", *Phys. Rev. B*, **53**, 8363.

Bhatia, M.A., Solanki, K.N., Moitra, A. and Tschopp, M.A. (2011), "The effect of crystallographic orientation on void growth: A molecular dynamics study", *Min. Metal. Mat. Soc. ASM Int*., **44A**, 617-626.

Bringa, E.M., Traiviratana, S. and Meyers, M.A. (2010), "Void initiation in fcc metals: Effect of loading orientation and nanocrystalline effects", *Acta Materialia*, **58**, 4458-4477.

Clarke, A.S. and Jónsson, H. (1993), "Structural changes accompanying densification of random hard-sphere packings", *Phys. Rev. E*, **47**, 3975.

Dantuluri, V., Maiti, S., Geubelle, P.H., Patel, R. and Kilic, H. (2007), "Cohesive modeling of delamination in Z-pin reinforced composite laminates", *Comp. Sci. Tech*., **67**(3-4), 616-631.

Daw, M.S. and Baskes, M.I. (1984), "Embedded-atom method: Derivation and application to impurities, surfaces, and other defects in metals", *Phys. Rev. B*, **29**, 6443-6453.

Dugdale, D.S. (1960), "Yielding of steel sheets containing slits", *J. Mech. Phys. Solid*., **8**, 100-104.

Faken, D. and Jonsson, H. (1994), "Systematic analysis of local atomic structure combined with 3D computer graphics", *Comput. Mater. Sci*., **2**, 279-586.

Ganesh, P. and Widom, M. (2006), "Signature of nearly icosahedral structures in liquid and supercooled liquid copper", *Phys. Rev. B*, **74**, 134205.

Garrison, W.M. Jr. and Moody, N.R. (1987), "Ductile fracture", *J. Phys. Chem. Solid*., **48**, 1035-1074.

Garzón, I.L. and Amarillas, A.P. (1996), "Structural and vibrational analysis of amorphous Au 55 clusters", *Phys. Rev. B*, **54**, 11796.

Griffith, A.A. (1921), "The phenomena of rupture and flow in solids", *Phil. Trans. R. Soc. Lond. A*, **221**, 163-198.

Holland, D. and Marder, M. (1999), "Cracks and atoms", *Adv. Mater*., **10**(11), 793-806.

Honeycutt, J.D. and Andersen, H.C. (1987), "Molecular dynamics study of melting and freezing of small Lennard-Jones clusters", *J. Phys. Chem*., **91**(19), 4950-4963.

Hoover, W.G. (1985), "Canonical dynamics: equilibrium phase-space distributions", *Phys. Rev. A*, **31**, 1695-1697.

Horstemeyer, M.F. and Baskes, M.I. (1999), "Atomistic finite deformation simulations: a discussion on length scale effects in relation to mechanical stresses", *ASME Tran. J. Eng. Mater. Tech*., **121**, 114-119.

Irwin, G.R. (1948), "Fracture dynamics", *Proceedings of the ASM Symposium on Fracturing of Metals*, Cleveland, OH.

Irwin, G.R. (1956), "Plastic zone near a crack and fracture toughness", *Proceedings of the Sagamore Conference on Strength Limitations of Metals*, NY Syracuse University Press, **2**, 289-305.

Irwin, G.R. (1957), "Analysis of stresses and strain near the end of a crack traversing a plate", *Tran. ASME Ser. E: J. Appl. Mech*., **24**, 361-364.

Jakse, N. and Pasturel, A. (2004), "Ab initio molecular dynamics simulations of local structure of supercooled Ni", *J. Chem. Phys*., **120**(13), 6124-6127.

Jónsson, H. and Andersen, H.C. (1988), "Icosahedral ordering in the Lennard-Jones liquid and glass", *Phys. Rev. Lett*., **60**, 2295.

Krull, H. and Yuan, H. (2011), "Suggestions to the cohesive traction–separation law from atomistic simulations", *J. Eng. Fract. Mech*., **78**, 525-533.

Kubair, D.V., Geubelle, P.H. (2003), "Comparative analysis of extrinsic and intrinsic cohesive models of dynamic fracture", *Int. J. Solid. Struct*., **40**, 3853-3868.

LAMMPS (2013), http://www.cs.sandia.gov/~sjplimp/lammps.html

Li, T.X., Yin, S.Y., Ji, Y.L., Wang, B.L., Wang, G.H. and Zhao, J.J. (2000), "A genetic algorithm study on the most stable disordered and ordered configurations of Au 38-55", *Phys. Lett. A*, **267**(5-6), 403-407.

Liu, X.Y., Ercolessi, F. and Adams, J.B. (2004), "Aluminium interatomic potential from density functional theory calculations with improved stacking fault energy", *Model. Simul. Mater. Sci. Eng*., **12**, 665-670.
McClintock, F.A. (1968), "A criterion for ductile fracture by the growth of holes", *J. Appl. Mech.*, **35**(2), 363-371.
Needleman, A. (1987), "A continuum model for void nucleation by inclusion debonding", *J. Appl. Mech*., **54**, 525-531.
Needleman, A. (1990), "An analysis of decohesion along an imperfect interface", *Int. J. Fract*., **42**, 21-40.
Nose, S. (1984), "A unified formulation of the constant temperature molecular dynamics methods", *J. Chem. Phys*., **81**, 511-519.
Paliwal, B. and Cherkaoui, M. (2013), "An improved atomistic simulation based mixed-mode cohesive zone law considering non-planar crack growth", *Int. J. Solid. Struct*., **50**, 3346-3360.
Plimpton, S. (1995), "Fast parallel algorithms for short-range molecular dynamics", *J. Comput. Phys*., **117**, 1-19.
Potirniche, G.P., Horstemeyer, M.F., Wagner, G.J. and Gullett, P.M. (2006), "A molecular dynamics study of void growth and coalescence in single crystal nickel", *Int. J. Plast*., **22**, 257-278.
Ren, G.W., Tang, T.G. and Li, Q.Z. (2012), "Atomistic study of anisotropic effect on two-dimensional dynamic crack", *Front. Mater. Sci*., **6**(1), 87-96.
Rice, J.R. and Rosengren, G.F. (1968), "Plane strain deformation near a crack tip in a power-law hardening material", *J. Mech. Phys. Solid*., **16**, 1-12.
Rösch, F., Trebin, H.R. and Gumbsch, P. (2006), "Fracture of complex metallic alloys: An atomistic study of model systems", *Phil Mag*., **86**, 1015-1020.
Le Roy, G., Embury, J.D., Edwards, G. and Ashby, M.F. (1981), "A model of ductile fracture based on the nucleation and growth of voids", *Acta Metallurgica*, **29**, 1509-1522.
Schiøtz, J., DiTolla, F.D. and Jacobsen, K.W. (1998b), "Softening of nanocrystalline metals at very small grain sizes", *Nature*, **391**, 561-563.
Schiøtz, J., Vegge, T., DiTolla, F.D. and Jacobsen, K.W. (1999), "Atomic-scale simulations of the mechanical deformation of nanocrystalline metals", *Phys. Rev. B*, **60**, 11971.
Sørensen, M.R., Brandbyge, M. and Jacobsen, K.W. (1998a), "Mechanical deformation of atomic-scale metallic contacts: structure and mechanisms", *Phys. Rev. B*, **57**, 3283.
Swope, W.C., Andersen, H.C., Berens, P.H. and Wilson, K.R. (1982), "A computer simulation method for the calculation of equilibrium constants for the formation of physical clusters of molecules: application to small water clusters", *J. Chem. Phys*., **76**, 637-649.
Tai, W.H. and Yang, B.X. (1986), "A new microvoid-damage model for ductile fracture", *Eng. Fract. Mech*., **25**, 377-384.
Thomason, P.F. (1998), "A view on ductile-fracture modelling", *Fatig. Fract. Eng. Mater. Struct*., **21**(9), 1105-1122.
Tomar, V., Zhai, J. and Zhou, M. (2004), "Bounds for element size in a variable stiffness cohesive finite element model", *Int. J. Numer. Meth. Eng*., **61**, 1894-1920.
Tvergaard, V. (2001), "Crack growth predictions by cohesive zone model for ductile fracture", *J. Mech. Phys. Solid*., **49**, 2191-2207.
Westergaard, H.M. (1939), "Bearing pressures and cracks", *J. Appl. Mech*., **6**, 49-53.
Williams, M.L. (1957), "On the stress distribution at the base of a stationary crack", *Trans. AMSE J. Appl. Mech*., **24**, 109-114.
Wu, W. and Yao, Z. (2012), "Molecular dynamics simulation of stress distribution and microstructure evolution ahead of a growing crack in single crystal nickel", *J. Theo. Appl. Fract. Mech*., **62**, 67-75.
Xu, S. and Deng, X. (2008), "Nanoscale void nucleation and growth and crack tip stress evolution ahead of a growing crack in a single crystal", *Nanotechnology*, **19**, 115705.
Xue, L. and Wierzbicki, T. (2008), "Ductile fracture initiation and propagation modeling using damage plasticity theory", *J. Eng. Fract. Mech*., **75**, 3276-3293.
Yamakov, V., Saether, E., Phillips, D.R. and Glaessgen, E.H. (2006), "Molecular-dynamics simulation-based cohesive zone representation of intergranular fracture processes in aluminum", *J. Mech. Phys.*

Solid., **54**, 1899-1928.
Yamakov, V., Wolf, D., Phillpot, S.R., Mukherjee, A.K. and Gleiter, H. (2002), "Dislocation processes in the deformation of nanocrystalline aluminium by molecular-dynamics simulation", *Nature Mater*., **1**(1), 45-49.
Yavari, A.R., Lewandowski, J.J. and Eckert, J. (2007), "Mechanical properties of bulk metallic glasses", *Mrs Bull.*, **32**(08), 635-638.
Zeng, X. and Li, S. (2010), "A multiscale cohesive zone model and simulations of fractures", *Comput. Meth. Appl. Mech. Eng*., **199**, 547-556.
Zhou, X.W., Moody, N.R., Jones, R.E., Zimmerman, J.A. and Reedy, E.D. (2009), "Molecular-dynamics-based cohesive zone law for brittle interfacial fracture under mixed loading conditions: effects of elastic constant mismatch", *Acta Materialia*, **57**(16), 4671-4686.
Zhou, M. (2003), "A new look at the atomic level virial stress: on continuum-molecular system equivalence", *Proc. R. Soc. London A*, 459, 2347-2392.
Zhou, X.W., Zimmerman, J.A., Reedy, E.D. and Moody, N.R. (2008), "Molecular dynamics simulation based cohesive surface representation of mixed mode fracture", *Mech. Mater*., **40**, 832-845.

CC